Feedback Control of Unsupported Standing in Paraplegia—Part I: Optimal Control Approach

Kenneth J. Hunt, Marko Munih, *Member, IEEE,* and Nick de N. Donaldson

***Abstract*—This is the first of a pair of papers which describe an investigation into the feasibility of providing artificial balance to paraplegics using electrical stimulation of the paralyzed muscles. By bracing the body above the shanks, only stimulation of the plantarflexors is necessary. This arrangement prevents any influence from the intact neuromuscular system above the spinal cord lesion. In this paper, we extend the design of the controllers to a nested-loop LQG (linear quadratic Gaussian) stimulation controller which has ankle moment feedback (inner loops) and inverted pendulum angle feedback (outer loop). Each control loop is tuned by two parameters, the control weighting and an observer rise-time, which together determine the behavior. The nested structure was chosen because it is robust, despite changes in the muscle properties (fatigue) and interference from spasticity.**

***Index Terms*—Artificial balance, feedback control, optical control, paraplegia, unsupported standing.**

I. Introduction

A. Purpose

OUR objective is to provide paraplegics with systems which will enable them to stand using functional electrical stimulation (FES). To provide satisfactory systems, one of the major areas of study must be that of control: how should the stimulator be modulated so as to optimize performance? The conventional view of this problem is that the requirement for the controller will be expressed in terms of the motions of all the joints: perhaps following trajectories or maintaining angles.

B. General Framework

When a paraplegic stands, there are three influences which will together determine the joints' motion: the effect of the FES on the leg muscles; the largely unpredictable spasticity, perhaps resulting in muscle spasms, due to the activity of the isolated lower spinal cord; and lastly, the actions of the neurologically intact upper-body. The upper body includes organs of balance, vision and, presumably, some useful proprioceptive and mechano-receptive sensations from the margins of sensations in the abdomen. Standing can be supported, in which case one or both hands hold some handle for balance, for sensory to the intact neuromuscular system (INS), and, if necessary, help lift the body weight. In this case the influence of the upper body on the leg joints is due to the fact that the body is then a closed kinematic chain [1]. Alternatively, the standing can be unsupported, in which case the kinematic chain is open and the influence of the upper body will be by dynamic coupling.

When there is no influence from the INS, the system can be regarded as a servo-controller problem for which the purpose is to make the joint angles closely follow some input trajectories. In its most simplified form, experiments can be done by stimulating isolated nerve-muscle preparations and measuring the joint moment or tendon force (e.g., [2]). Even

Fig. 1. The wobbler apparatus with paraplegic subject.

Manuscript received June 10, 1997; revised September 14, 1997.

K. J. Hunt is with Daimler-Benz AG, Alt-Moabit 96 A, Berlin, Germany.

M. Munih is with the Faculty of Electrical Engineering, University of Ljubljana, Ljubljana, Slovenia.

N. de N. Donaldson is with the Department of Medical Physics and Bioengineering, University College London, London WC1E 6JA U.K.

Publisher Item Identifier S 1063-6528(97)08931-3.

such simplified systems are of interest because of the many well-known properties of the stimulated nerve-muscle-joint which make control difficult. A partial list is as follows:

- the nonlinear response to recruitment [3];
- the nonlinear response to inter-pulse interval [4], [5];
- the transmission delay for the action potentials to travel from the electrode to the muscle and the low-pass frequency characteristic of the muscle [6];
- the changes in force and frequency response due to potentiation [7] and fatigue [8];
- the dependence of the joint moments on the joint angles (muscle lengths) and joint velocities [9]; and
- the existence of bi-articular muscles.

If a controller can be designed which is satisfactory despite these difficulties, the effects of spasticity can be thought of as unpredictable disturbances to the output, due to spasm [10], or to the joint stiffness, if spasticity is manifested as an increased rigidity of the joint [11].

In clinical tests of controllers, the INS can influence the motion of the leg joints, and therefore tests do not show how well the control mechanisms in the joints perform. For example, if trajectory-tracking was the goal but a large mean angular error occurred, without special instrumentation one can not know whether this is due to poor tracking performance of the stimulated muscle controller, spasticity, or a significant effect from the upper body. This problem will occur whether the controllers are conventional servos, finite state controllers, fuzzy controllers, or any other type which only uses feedback from the legs. A fundamental shortcoming of this type of artificial controller is that it does not automatically act in a coordinated way with the INS. Ideally, the artificial controller should behave as an integral part the natural postural controller.

It is, however, valuable to know how well artificial controllers can work with paraplegics when the INS has no influence, because of the difficulties of using nerve-muscle-joint as an actuator. Furthermore, it seems to us to be desirable that this should be tested with a realistic postural task. In the work, of which this pair of papers describes part, the task is to achieve artificial balance by stimulating the plantarflexors. By strapping the paraplegic volunteer into a brace which extends from his calves to his head, the knee- and hip-extensors need not be stimulated but also the upper body is restrained (Fig. 1). The subjects were asked to keep their arms still (folded across the chest was one preference) and the body, which can then be approximated as a single-link inverted pendulum, is prevented from falling (when the controller fails to maintain balance) by four slightly slack ropes which run to secure cleats on a frame below the ceiling [12]. (In Fig. 1, two ropes, which are dark-colored, can be seen, here taught, running forward and backward, and each slightly laterally, from the subject's right shoulder. A similar pair of ropes in on his left side.)

C. Related Work and Literature

The question of whether the plantarflexors of paraplegics might be used with servo-controllers to provide artificial balance has been investigated by Trnkoczy *et al.* [13] and by Bajzac and Jaeger [14]. Neither of these groups could test their controllers with the plant except by what we term Actual Standing; they could not test the stiffness of the joints nor could they apply a repeatable displacement to test the controllers, as is possible with our apparatus. Robinson *et al.* [15] and Sinkjaer *et al.* [16] did make apparatus for looking at the stiffness of the ankles of paraplegics, and this allowed the passive and reflex stiffness effects to be distinguished, however, it was not used with feedback control. An overview of closed-loop control in functional electrical stimulation is given by Chizeck [17].

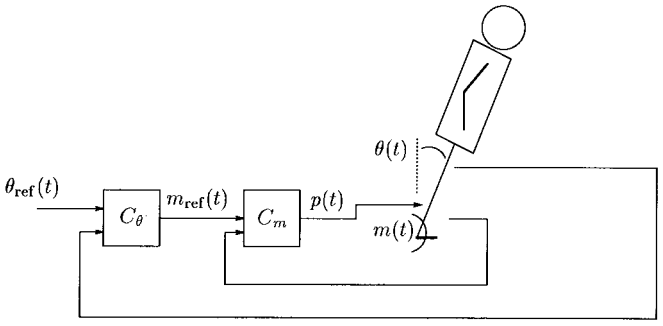

Fig. 2. Feedback control of unsupported standing: θ: measured ankle angle, m: measured ankle moment, p: muscle stimulation (constant amplitude and frequency, variable width pulses), θ_{ref}: angle set-point, m_{ref}: moment set-point, C_θ: angle controller, and C_m: moment controller.

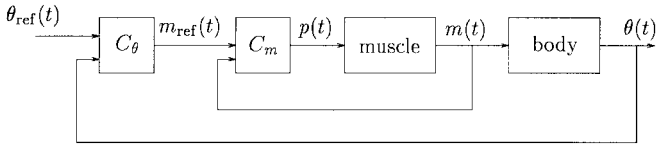

Fig. 3. Nested control structure for unsupported standing.

D. Our Approach and Results

Our approach to the problem began with the realization that the actuators (muscles) were more variable and have shorter time constants than the inverted pendulum (body) and therefore that a more robust controller would use negative feedback of the joint moments [18]. This led to the three-loop nested structure described below (Figs. 2 and 3). However, given the separate loops, the possibility presented itself, that we could assess the performance of the inner loops in dynamic tests before embedding them inside the angle-control loop. To perform these dynamic tests, the "Wobbler" was devised, apparatus which could not only be used in isometric tests but also in three possible dynamic tests: sinusoidal stiffness measurement without any feedback to the stimulator; moment control loop testing with sinusoidal displacement; and Imitation Standing in which all the control structure is tested but with the outer loop open and the subject secure.

In previous papers in the series, we have reported on the Wobbler apparatus [12], the stiffness characteristics of the ankle [11], the design of optimal controllers for isometric ankle moment [19] and the shortcomings of using the Hammerstein structure to represent the isometric muscle [20]. This paper deals with optimal controller design for balancing the inverted

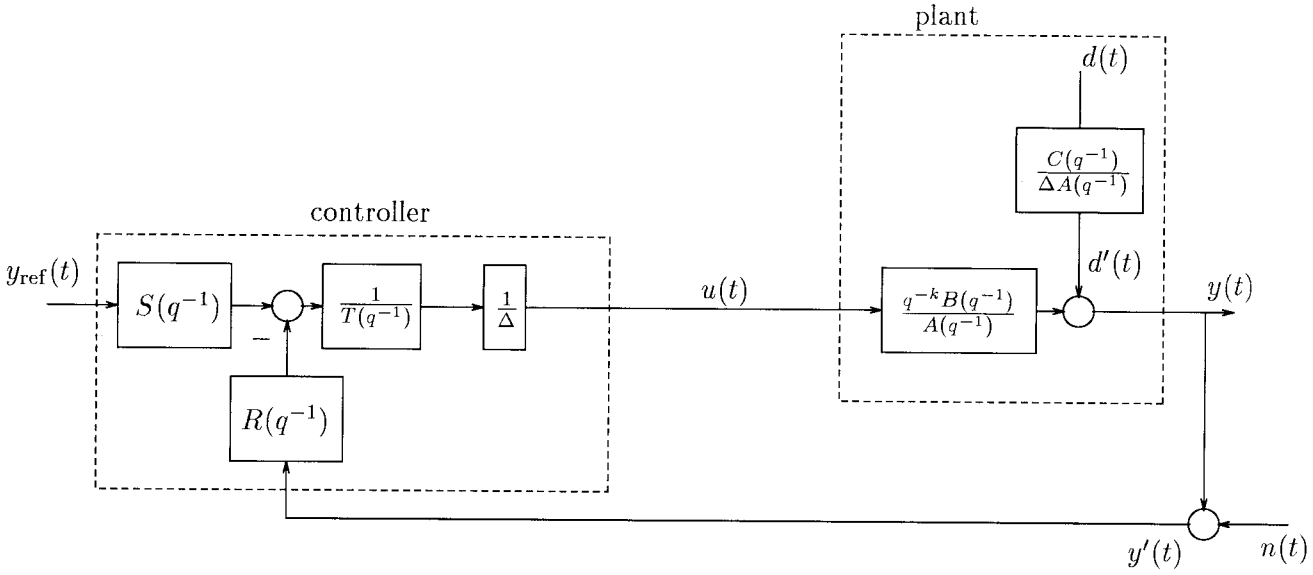

Fig. 4. Generic feedback control system, $\Delta = 1 - q^{-1}$: y: plant output (to be controlled), $y_{\rm ref}$: desired output (reference), u: control signal, d: net disturbance effect, n: measurement noise.

pendulum. The sequel [21] presents experimental results obtained from an intact and a paraplegic subject in the Wobbler, in which balance, when it occurred, was largely due to the action of the artificial controller (see Discussion in Part II of this paper).

II. Control Strategy for Unsupported Standing

A. Measurable Signals and Nested Controllers

The system to be controlled consists of the biomechanical dynamics of the rigid body, and part of the paralyzed neuromuscular system; the muscles serve as actuators for positioning the body. In the experimental setup, as described in Part II of this paper, we are able to measure both the muscle-produced moment and the angle of the body (see Fig. 3). The inner loop of the nested control structure provides feedback control of muscle moment, and the outer loop controls the angle. Due to the time constants involved, the inner loop can have a much higher bandwidth than the outer loop. This provides the benefit that the uncertain effects of muscle nonlinearity and time variation are reduced. The nested control structure is shown schematically in Fig. 3.[1]

B. Generic Feedback Loop and Optimal Control Design Solution

The control design approach involves first designing the inner loop controllers based upon empirically-derived muscle models. The outer loop is then designed, taking account both of the inner closed-loop and the body dynamics in the outer loop. In this paper, we use linear optimal control theory to design the controllers. The nonlinear muscle is described in Hammerstein form with a static input nonlinearity followed by a linear transfer function. In the inner-loop controllers the nonlinearity is approximately cancelled using the inverse of an estimated static nonlinearity.

The controllers for both loops have an identical two-degrees-of-freedom feedback structure; a generic two-degrees-of-freedom feedback structure is depicted in Fig. 4 and the design procedure for both loops can best be explained with reference to this. For the inner loop controller the "plant" is the muscle, while for the outer loop controller the plant is the combination of inner-loop dynamics and the biomechanical dynamics.

In the generic structure, the control signal u drives the plant transfer-function $q^{-k}B(q^{-1})/A(q^{-1})$. Here, the integer $k \geq 1$ is a discrete input–output time-delay, while A and B are polynomials in the delay operator q^{-1} and have the form

$$A(q^{-1}) = 1 + a_1 q^{-1} + \cdots + a_{na} q^{-na} \tag{1}$$

$$B(q^{-1}) = b_0 + b_1 q^{-1} + \cdots + b_{nb} q^{-nb}. \tag{2}$$

The net effect of disturbances is represented at the output by the signal d driving the filter $C(q^{-1})/(1 - q^{-1})A(q^{-1})$. The integrating term $\Delta = 1 - q^{-1}$ is included in the plant's disturbance path to model the effect of stepwise-changing (piecewise-constant) disturbances and offsets, which are typical due to the muscle physiology, and which also depend on the operating point.[2] The idealized assumption of piecewise-constant disturbances approximates the true situation where some of the disturbances and system parameters are slowly time-varying. A major source of disturbance is due to muscle stiffness [11], [19]; low-frequency sway in standing appears as a slowly-varying disturbing moment at the ankle. In addition to this, the system parameters vary slowly due to fatigue.

[1] Note that there are in fact two inner loop moment controllers, one for each ankle. For the purposes of exposition, we assume here that both sides are incorporated into the controller C_m.

[2] Such nonstationary disturbances can be represented in the stochastic framework by considering d to be a compound or generalized Poisson process, i.e. a sequence consisting of random pulses of variable magnitude occuring at random times. See [22] for details.

Here, 'slowly' should be interpreted with respect to the system time-constants.

Generically, the open-loop plant can be represented by the model

$$y(t) = \frac{q^{-k}B(q^{-1})}{A(q^{-1})}u(t) + \frac{C(q^{-1})}{(1-q^{-1})A(q^{-1})}\,d(t). \quad (3)$$

The output to be controlled $y(t)$ is corrupted by a measurement noise n so that the signal

$$y'(t) = y(t) + n(t) \quad (4)$$

is available for feedback. In this formulation, the disturbance and measurement noise signals d and n are modeled as mutually uncorrelated zero-mean stochastic signals with intensities ψ_d and ψ_n, respectively.

Since the input–output paths of both the muscle and the biomechanical dynamics contain no inherent integrating behavior, and since the disturbances for both loops contain approximately piecewise-constant offsets, an integrator must be incorporated in both the inner and outer-loop controllers. This is represented by the integrating term $1/\Delta$ in the controller, with $\Delta = 1 - q^{-1}$, in Fig. 4. Each controller has a two-degrees-of-freedom form, so that the reference tracking behavior can be influenced independently of the feedback loop properties, and is described by

$$u(t) = \frac{1}{(1-q^{-1})T(q^{-1})}(S(q^{-1})y_{\rm ref}(t) - R(q^{-1})y'(t)) \quad (5)$$

where S, R and T are polynomials in the delay operator. The polynomials T and R are determined in the optimization procedure, and correspond to the analytical solution of the optimal regulator problem (i.e., for the case $y_{\rm ref} = 0$). The choice of S for the tracking problem $(y_{\rm ref} \neq 0)$ is discussed below.

The optimization cost-function used for each loop is chosen to allow a simple tradeoff between output variance and control variable activity. A suitable way of achieving this aim is to minimize the LQG[3] cost function

$$J = \epsilon\Big[y^2(t) + \rho\big((1-q^{-1})u\big)^2(t)\Big] \quad (6)$$

where ϵ is the expectation operator and $\rho > 0$ is the tuneable control weighting. The control weighting is a design parameter which serves as one of the controller "tuning knobs" (see Section V). Due to inclusion of integral action via the $1-q^{-1}$ term, it is the increments in the control signal u which are penalized. This will ensure there is no steady-state tracking error.

A formal solution to this optimization problem, including underlying assumptions and solvability conditions, can be found in the references [23] and [22]; the design equations resulting from the analytical solution are informally stated here. First, two polynomials D_c and D_f are computed. These are the stable solutions to the spectral factorizations[4]

$$D_c D_c^* = BB^* + \big(1-q^{-1}\big)A\rho A^*(1-q) \quad (7)$$

$$D_f D_f^* = C\psi_d C^* + (1-q^{-1})A\psi_n A^*(1-q). \quad (8)$$

[3] linear quadratic Gaussian.

[4] For any polynomial $X(q^{-1})$ we define $X^*(q^{-1}) = X(q)$.

Stable solutions for D_c and D_f exist when A and B have no unstable common factors. The controller polynomials T and R which correspond to the minimal value of the cost-function (6) are obtained from the solution of the linear polynomial equation

$$(1-q^{-1})AT + q^{-k}BR = D_f D_c \quad (9)$$

subject to the condition

$$\big((1-q^{-1})A\big)^{-1}R \text{ strictly proper} \quad (10)$$

i.e., $\deg(R) < \deg(A) + 1$. A sufficient condition to ensure existence of a unique solution with this property is that the polynomials A and B have no common factors.

Note that this optimal control problem has an equivalent solution in a state-space formulation of the LQG problem [24]. The *control* spectral factor D_c corresponds to the poles of the control Ricatti equation, and the *filter* spectral factor D_f corresponds to the observer poles (the Kalman filter poles).

Servo performance (i.e., reference tracking) is defined by the transfer-function between $y_{\rm ref}$ and y, denoted as $G_{y/y_{\rm ref}}$. By considering the structure of Fig. 4 and employing (9) this transfer function is found to be

$$G_{y/y_{\rm ref}} = \frac{q^{-k}BS}{(1-q^{-1})AT + q^{-k}BR} = \frac{q^{-k}BS}{D_c D_f}. \quad (11)$$

The open-loop zeros appear in this expression since in general the optimal controller performs no zero cancellation within the loop[5]. It is important to introduce the reference signal in such a way that it does not excite the observer dynamics [25]. This is achieved by constraining S as

$$S(q^{-1}) = \lambda D_f(q^{-1}) \quad (12)$$

where λ is a scalar which is set to achieve unity steady-state gain in this closed-loop transfer-function. Combining (11) and (12) the closed-loop transfer-function becomes

$$G_{y/y_{\rm ref}}(q^{-1}) = \frac{\lambda q^{-k}B(q^{-1})}{D_c(q^{-1})} \quad (13)$$

and the appropriate value of λ is therefore

$$\lambda = D_c(1)/B(1). \quad (14)$$

The reference tracking properties of the system as defined by $G_{y/y_{\rm ref}}$ are effectively decoupled from measurement noise effects due to the constraint (12). One further option is to employ a prefilter which cancels the term D_c in (13) (D_c can be cancelled because it is by definition stable), and which introduces desirable tracking dynamics. This option is not pursued in this paper. The disturbance rejection and measurement noise sensitivity properties of the closed-loop are discussed later (see Section V), as are the trade-offs involved in the choice of the control design parameters.

[5] Cancellation of stable zeros could be arranged if desired by incorporating the zeros to be cancelled as factors of T.

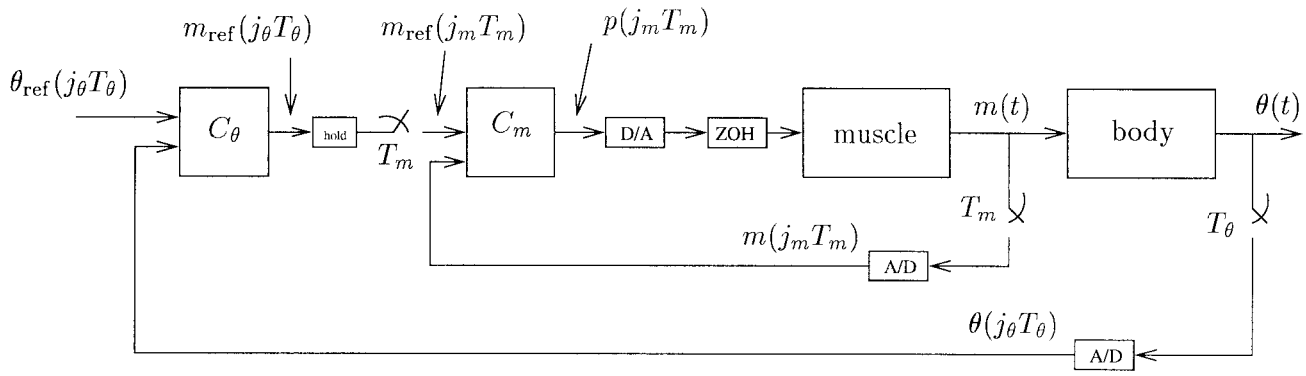

Fig. 5. Multirate sampling of feedback loops, j_θ and j_m are integer indexes. The Fig. shows A/D and D/A converters, zero-order hold (ZOH) elements, and samplers.

C. Multirate Sampling

For physiological reasons[6] the muscle stimulator operates at a rate of $f_m = 20$ Hz, and the sample period for the inner loop is therefore $T_m = 50$ ms.

As mentioned above, the muscle dynamics are much faster than the body dynamics. For this reason, the inner loop for muscle moment control can have a significantly higher bandwidth than the position control loop. This fact has implications for the choice of sampling rate for the inner and outer loops, since the sampling rate in a sampled-data control system should be related to the closed-loop bandwidth. Typically, the sampling rate should be chosen such that there are around 5–20 samples per closed-loop rise time [25].

Thus, the sampling rate for the muscle moment control loop can be higher than that for the position loop. Indeed, we have found that sampling the outer loop at the fast inner-loop rate leads to numerical sensitivity problems for position control, for reasons documented in the references [25], [26] and demonstrated in our experimental results. In our experimental setup the outer-loop sampling can be slower than, but is always synchronized with, inner-loop sampling, i.e., $T_\theta = \tilde{k} T_m$, where $\tilde{k}$ is an integer. Typically, we have used $\tilde{k} = 3$, giving an outer-loop sample period of $T_\theta = 150$ ms (a sample rate of $f_\theta = 6.7$ Hz).

A refined version of the nested controller structure of Fig. 3, in which the multirate sampling arrangement is shown in detail, is depicted in Fig. 5. The sampling rate for the position loop is denoted as T_θ, and that for the moment control loop as T_m. As will be seen in Section IV-C, detailed consideration of this sampling arrangement is required in the formulation of the design plant for the outer loop controller, as the plant in this case consists of the inner closed-loop dynamics combined with the continuous biomechanical dynamics.

D. Plant Definition for Outer (Position) Controller Design

Account must be taken of the multirate sampling arrangement in the definition of the "plant" seen by the position controller C_θ: this plant consists of all components between the position controller output (m_{ref}) and the body angle (θ). This situation is depicted in Fig. 6. The precise details involved in computation of the outer-loop design plant are given in Section IV-C.

[6] Stimulation frequencies at or close to 20 Hz are often used because this rate is high enough for the contraction to be acceptably smooth. The stimulation rate cannot however be much higher than this as then the high rate of muscle fatigue would be exacerbated.

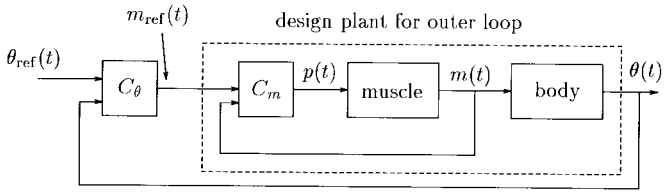

Fig. 6. Definition of the design plant for outer controller design.

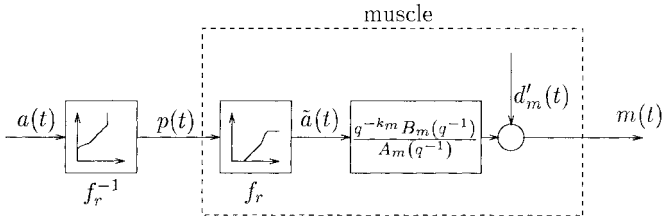

Fig. 7. Hammerstein model of muscle, showing structure for transfer-function identification, $d'_m(t) = d_m(t)/((1-q^{-1})A_m(q^{-1}))$.

III. Muscle Modeling and Ankle Moment Control

In this section we present the techniques used for modeling, identification and control design in the inner loop. A full presentation of issues relating to ankle muscle modeling and identification has been given in Hunt *et al.* [20], and ankle moment control was investigated in Hunt *et al.* [19]. Here, we outline the structures used, as this is required for the position loop design of Section IV, and we give some typical results.

A. Muscle Modeling and Identification

The muscle is represented in Hammerstein form as depicted in Fig. 7; it consists of a static recruitment nonlinearity f_r, followed by a discrete-time linear transfer function $q^{-k_m} B_m(q^{-1})/A_m(q^{-1})$. The sample period for the muscle loops is $T_m = 50$ ms. The linear part of the model has the generic structure given by (3), with $C(q^{-1}) = 1$, and the subscript m specialises the generic situation to the muscle. The signal $\tilde{a}$ is a notional muscle "activation level." As described

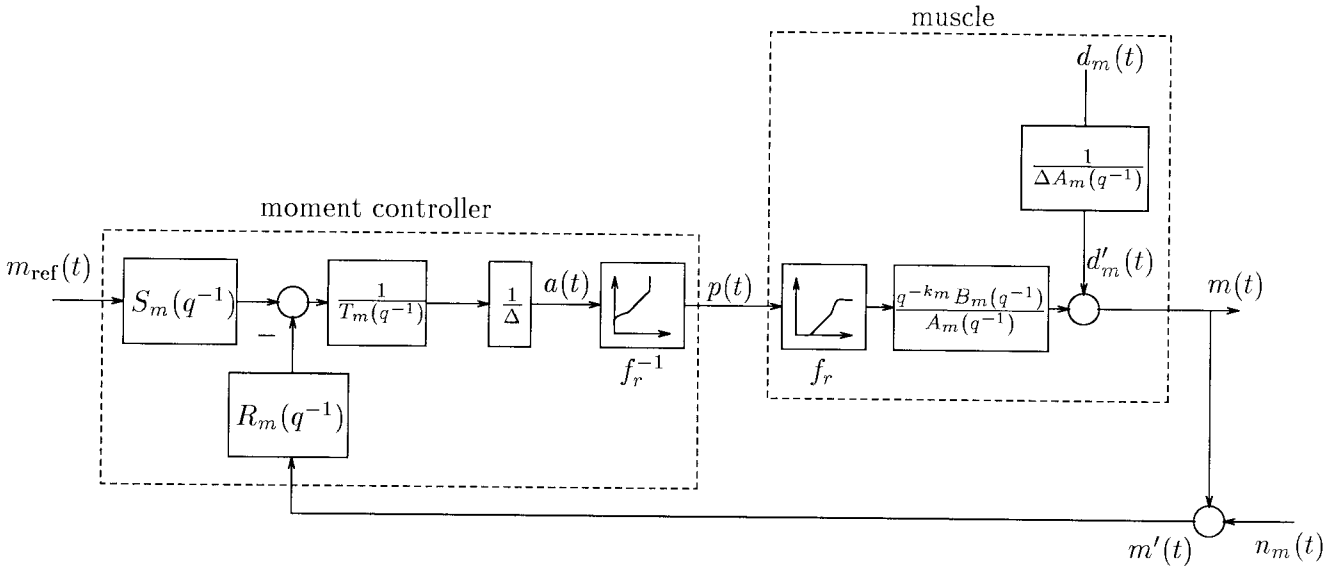

Fig. 8. Closed-loop system for muscle moment control, $\Delta = 1 - q^{-1}$. The sampling interval for this loop is T_m.

in [20], empirical determination of the Hammerstein model consists of two steps:

1) the impulse response method [3] is used to determine the recruitment nonlinearity f_r based on twitch response data (the responses to well-separated stimulus pulses from which the muscle contraction or twitch is completed before the next stimulus pulse);
2) having obtained the recruitment nonlinearity, parametric identification methods are used to determine the parameters of the linear transfer-function. Typically, a pseudo-random binary sequence (PRBS)-stimulation test is employed to generate identification data. In the PRBS test, the recruitment nonlinearity is first cancelled via its inverse f_r^{-1}, using the structure of Fig. 7. The signal $a(t)$ is the desired muscle activation, which is normalized to the range from 0 to 1000 mAct (we define 1000mAct as full activation of the ankle plantarflexor muscles).

B. Moment Control

The feedback loop for muscle moment control is based upon the generic structure defined above. However, the inner loop takes direct account of the Hammerstein structure of the muscle model by incorporating an approximate inverse of the recruitment nonlinearity at the controller output. The muscle moment control loop is shown in Fig. 8. The subscript $_m$ in the figure specialises the generic control loop of Fig. 4 to the muscle (with $C = 1$). The cost function for moment control is [cf., (6)]

$$J = \epsilon[m^2(t) + \rho_m((1 - q^{-1})a)^2(t)] \tag{15}$$

where ϵ is the expectation operator and $\rho_m > 0$ is the tuneable control weighting. Due to inclusion of integral action via the Δ term, it is in fact the increments in activation Δa which are penalized. The disturbance and noise intensities for this loop are ψ_{d_m} and ψ_{n_m}.

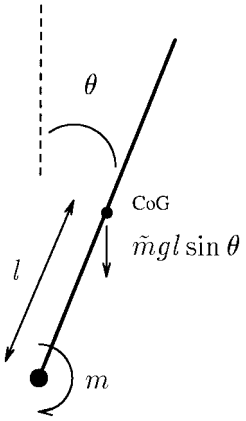

Fig. 9. Biomechanical system. CoG—Center of Gravity.

Computation of the moment controller polynomials S_m, R_m, and T_m requires solution of the spectral factorizations (7)–(8), with appropriate substitution of the muscle's plant and control design parameters. Equation (9) is then solved for R_m and T_m. S_m is obtained from (12) and (14).

The feedback action of the moment controller provides a certain level of robustness against uncertainty in the muscle model. Following control design, the stability margins (gain and phase margins) are checked to ensure a sufficient degree of robustness.

IV. Stabilization of Body Angle

In contrast to the neuromuscular system, the biomechanical dynamics can be relatively easily modeled, and we outline a simple method for experimental determination of the key variables in the model: the body mass and moment of inertia. Once measured, these parameters will not vary significantly during an experimental session provided the arms and head are not moved; the other body segments are braced. For a given subject the parameters will vary only slowly over longer periods of time.

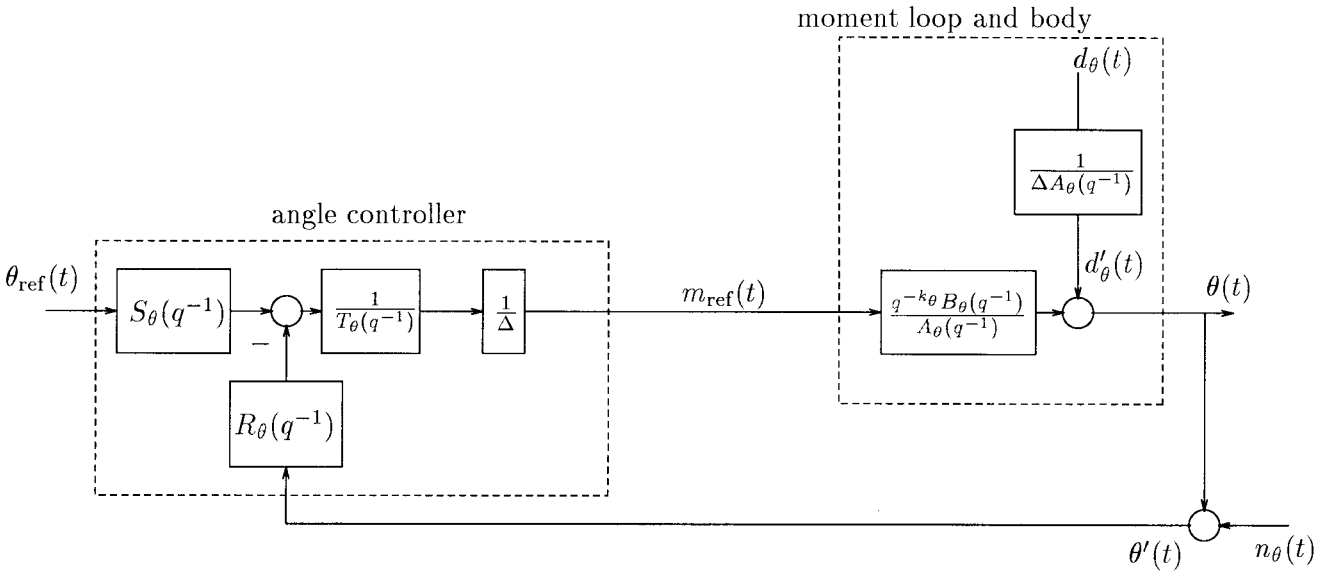

Fig. 10. Closed-loop system for body angle control. The sampling interval for this loop is T_θ. The plant in this case consists of the closed loop formed by the muscle and moment controller, cascaded with the biomechanical dynamics: $\theta_{\rm ref}$—desired angle (setpoint) and $m_{\rm ref}$—required moment.

A. Biomechanical Model of Standing

The equation of motion of the rigid body dynamics, free only to move about the ankle, and maintained upright by a variable moment m about the ankle, is (see Fig. 9)

$$m + \tilde{m}gl\sin\theta = J\frac{d^2\theta}{dt^2}. \tag{16}$$

In this equation, $\tilde{m}$ is the mass and J is the moment of inertia. The centre of gravity is assumed to be at length l (g is the acceleration due to gravity). For small angles of inclination we have $\sin\theta \approx \theta$ and the linearized transfer-function of the body dynamics is

$$\frac{\Theta(s)}{M(s)} = \frac{1/J}{s^2 - \tilde{m}gl/J} \tag{17}$$

where s is the Laplace-transform complex variable, and capital letters indicate transformed signals.

B. Identification of Body Parameters

The biomechanical variables $\tilde{m}, l$ and J were determined experimentally while the subject was strapped into the plastic half-shell which made his body rigid above the ankles [12]. While in the shell, the body was lifted onto weighing scales, so that it was supported under the legs and trunk. From the positions of the scales and the measured weights, the mass and centre of mass were found. The moment of inertia was calculated from the resonant frequency of the body, while pivoted at the ankles, and suspended from a long spring, attached at the chest.

The intact subject in the experiments reported in Part II was aged 43, had height 170 cm, mass $\tilde{m} = 70$ kg and inertia $J = 88.7$ kgm^2. The paraplegic subject has a complete T5 lesion, is aged 35 years, is 13 years after injury, has height 175 cm, mass $\tilde{m} = 75$ kg, and inertia $J = 95$ kgm^2.

C. Position Control Design

The multirate sampling structure for the nested control loops was described in Section II-C (see Fig. 5), and account must be taken of this in the definition of the 'plant' seen by the position controller C_θ (see Fig. 6). Computation of this plant consists of three steps:

1) the closed-loop transfer-function of the inner loop (consisting of the muscle and the moment controller), given by (13) as $\lambda_m q^{-k_m} B_m(q^{-1})/D_c^m(q^{-1})$, is transformed to the continuous-time domain using the sample rate T_m;
2) the continuous inner-loop transfer-function thus obtained is cascaded with the continuous body dynamics $\Theta(s)/M(s)$ from (17);
3) the combined inner loop and body dynamics are transformed to discrete time using the sample rate T_θ. We denote the resulting discrete transfer-function as $q^{-k_\theta}B_\theta(q^{-1})/A_\theta(q^{-1})$; this is the plant used for position-loop design.

Based on these transformations, which are performed automatically using the `c2dm` and `d2cm` functions in MATLAB, the outer loop of Fig. 5 simplifies for the purposes of angle controller design and analysis to the structure shown in Fig. 10. We assume a similar structure for disturbance and noise effects as before, with appropriate notational changes, and we choose the noise polynomial $C(q^{-1})$ from the generic plant (3) to be $C = 1$.

A suitable cost function for angle control is [c.f. (6)]

$$J = \epsilon[\theta^2(t) + \rho_\theta((1-q^{-1})m_{\rm ref})^2(t)]. \tag{18}$$

In this case the control signal is the desired moment which is fed to the inner-loop controller. Due to inclusion of integral action via the Δ term, it is in fact the increments in desired moment $\Delta m_{\rm ref}$ which are penalized. For the angle control loop the disturbance and noise intensities are denoted as ψ_{d_θ} and ψ_{n_θ}

The generic control design equations can now be readily specialized to the angle loop. The regulator polynomials T_θ and R_θ which correspond to the minimal value of the cost-function (18) are obtained from the solution of the linear polynomial equation (9), with appropriate substitution of the plant's parameters. The spectral factors in (9) are obtained by solving (7)–(8). S_θ is obtained from (12) and (14).

V. Feedback Loop Properties and Design Parameters

A. Effect of Design Parameters

The parameters which affect the calculation of the optimal controllers for inner and outer loops are the control weighting ρ, and the intensities of the disturbance and measurement noise signals ψ_d and ψ_n. Since these intensities are difficult to determine accurately they can be considered, along with ρ, as control design parameters. Since from (8) it is merely the relative values of ψ_d and ψ_n which determine D_f, it may be assumed without loss of generality that $\psi_d = 1$. Thus, there are two scalar control design parameters for each moment control loop and two for the position loop: control weighting ρ and measurement noise intensity ψ_n.

The effect of varying ρ_m and ρ_θ can be seen clearly from the cost-function definitions (15) and (18). Higher values of ρ will penalise changes in the control signal (i.e., muscle activation or moment reference) more strongly, and the variance of the output (i.e., muscle moment or angle) will be correspondingly higher. In frequency domain terms, higher ρ will reduce the bandwidth of the closed-loop resulting in poorer disturbance rejection, but less sensitivity to measurement noise. The qualitative effect of changes in ρ on reference tracking is the same, i.e., faster reference tracking is achieved with lower control weighting.

The effect of measurement noise intensity ψ_n can be seen from the filter spectral factorization (8) for D_f. It should be noted that the filter spectral factor corresponds to the observer poles in a state-space formulation of the regulator problem (see [27], [25]). As $\psi_n \to 0$, the feedback system effectively has a deadbeat observer since $D_f \to 1$ in this case (i.e. with $\psi_d = 1$ and $C = 1$). On the other hand, as ψ_n tends toward a large number, the observer poles tend to the poles of the open-loop system, which in the case of the ankle muscle has low-pass characteristics. The effect of increasing the noise intensity is thus to generate faster roll-off of the loop transfer-function. This will reduce sensitivity to measurement noise (for the control signal in particular) while generally leading to somewhat poorer disturbance rejection. As described in Section II-B, the controller setup is such that ψ_n has no effect on reference tracking speed [see (12)–(14)].

B. Alternative Selection of Observer Polynomial

An alternative method for the choice of the observer poles which avoids the spectral factorization (8) is based on the observation that increasing ψ_n leads to a low-pass characteristic with a dominant pair of poles (the muscle transfer-function is predominantly second order). The alternative is therefore to directly specify the observer poles to correspond to a second-order transfer-function with given time-domain properties, such as rise-time and damping. This method has been succesfully implemented for moment control. It is assumed that the desired damping factor is unity (critical damping) and only the rise-time, denoted t_{obs}, must be specified. This specification of rise-time and unity damping leads directly to an equivalent continuous-time transfer-function

$$\frac{\omega_n^2}{s^2 + 2\omega_n s + \omega_n^2} \tag{19}$$

where ω_n is the natural frequency associated with specified rise-time t_{obs} and unity damping factor. From a simple time-domain analysis of the second order system (19), ω_n can be shown to be related to t_{obs} through $\omega_n = 3.2/t_{\text{obs}}$. D_f is then given by the denominator of the discretized version of this transfer-function. Qualitatively, increasing t_{obs} has the same effect as increasing ψ_n. For the moment and angle control loops the observer rise-times are denoted, respectively, as t_{obs}^m and t_{obs}^θ.

The effects of varying the design parameters are summarized in Table I.

TABLE I
Effect of Varying Controller Design Parameters

	tracking speed	disturbance rejection	noise sensitivity
$\rho \uparrow$	slower	worse	better
$\rho \downarrow$	faster	better	worse
$\psi_n, t_{\text{obs}} \uparrow$	no change	worse	better
$\psi_n, t_{\text{obs}} \downarrow$	no change	better	worse

C. Controller Tuning

Tuning of all three controllers in the nested-loop configuration proceeds in a number of steps. First, the internal moment-control loops are adjusted by observing closed-loop reference tracking, disturbance rejection performance and the influence of measurement noise. In the moment controllers, given the muscle polynomials A_m and B_m as the output of muscle identification [20], the design parameters ρ_m (control weighting) and t_{obs}^m (observer rise-time) represent the "tuning knobs." During LQG controller design in MATLAB these design parameters are used together with the muscle A_m and B_m polynomials, and the chosen sampling frequency $T_m = 50$ ms, to obtain the controller polynomials R_m, S_m, and T_m. These are implemented later in a real-time program. The details of the moment controller design procedure, tuning, simulations and experimental results are explained in detail in reference [19]. From the functional point of view, the moment controllers in this specific application are required to give high disturbance rejection and good reference tracking. Measurement noise immunity, while important and requiring verification, is of secondary concern. Lowering the values of both ρ_m and t_{obs}^m gives increased rejection of disturbances

and less phase lag in reference tracking, but simultaneously increases measurement noise sensitivity. For this reason, measurement sensor resolution, sensor noise level, superimposed noise on connection and communication wires, and noise during quantization are all very critical for achieving high performance control. According to these limitations we found the range $0.00005 \leq \rho_m \leq 0.001$ and $0 \leq t^m_{\rm obs} \leq 0.4$ to be useful for ankle moment controller application, with the best performance achieved when using ρ_m values at the lower declared margin with a deadbeat observer (i.e. $t^m_{\rm obs} = 0$).

The position loop controller is the same LQG-type as the moment controllers, and thus has two tuning knobs, the control weighting ρ_θ and observer rise-time $t^\theta_{\rm obs}$. For the design of the position controller polynomials R_θ, S_θ, and T_θ it is possible either to neglect the inner loop dynamics (since they are much faster than those of the outer loop) or to directly include the inner closed-loop dynamics as part of the design "plant" (as described previously). The latter approach was found to give better performance. Following design of the position controller, it is very difficult to do reference tracking and disturbance rejection tests, and to tune the controller design parameters on-line. For this reason, rough values for ρ_θ and $t^\theta_{\rm obs}$ are obtained in simulations and then adjusted in "Imitation Standing" (see Part II), and finally these are used in Actual Standing experiments. The ranges $0.0001 \leq \rho_\theta \leq 0.1$ and $0 \leq t^\theta_{\rm obs} \leq 0.4$ were found to be useful. Tuning was first done on intact persons and later verified on paraplegics; the experimental results are fully described in Part II of the paper.

VI. Conclusions

We have presented a control methodology in which the plant is treated as two parts:

1) the muscle-actuators which are nonlinear and vary relatively quickly and
2) the inverted pendulum which is well understood and relatively constant.

Because of the variability of the muscle properties with time, a nested control structure is used. The high-bandwidth inner-loop controllers serve to neutralise the nonlinear effects of the muscles.

In the optimal control approach, two "tuning knobs" are required for each of the three control loops. The effect of changes in these Tuning Knobs on closed-loop performance (reference tracking, disturbance rejection and measurement noise sensitivity) has been described. Tuning and subsequent testing is done in the Wobbler apparatus. Computation of the three control signals at each sample instant has been experimentally determined to take 6–7 ms; this is negligible with respect to the stimulation rate of 20 Hz.

Experimental results of unsupported standing trials in intact and paraplegic subjects are presented in the companion paper [21].

References

[1] N. Donaldson and C.-H. Yu, "FES standing: Control by handle reactions of leg muscle stimulation (CHRELMS)," *Trans. IEEE Rehab. Eng.*, vol. 4, pp. 280–284, Dec. 1996.

[2] G. Wilhere, P. Crago, and H. Chizeck, "Design and evaluation of a digital closed- loop controller for the regulation of muscle force by recruitment modulation," *IEEE Trans. Biomed. Eng.*, vol. 32, pp. 668–676, Sept. 1985.

[3] W. K. Durfee and K. E. Maclean, "Methods of estimating the isometric recruitment curve of electrically stimulated muscle," *IEEE Trans. Biomed. Eng.*, vol. 36, pp. 654–667, 1989.

[4] F. Parmiggiani and R. B. Stein, "Nonlinear summation of contractions in cat muscles. II Later facilitation and stiffness changes," *J. Gen. Physiol.*, vol. 78, pp. 295–311, 1981.

[5] N. Donaldson, H. Gollee, K. J. Hunt, J. C. Jarvis, and M. K. N. Kwende, "A radial basis function model of muscle stimulated with irregular inter-pulse intervals," *Med. Eng. Phys.*, vol. 17, pp. 431–441, Sept. 1995.

[6] P. Bawa and R. Stein, "Frequency response of human soleus muscle," *J. Neurophysiol.*, vol. 39, pp. 788–793, 1976.

[7] T. Sinkjaer, N. Gantchev, and L. Arendt-Nielsen, "Mechanical properties of human ankle extensors after muscle potentiation," *Enceph. Clin. Neurophysiol.*, vol. 85, pp. 412–418, 1992.

[8] I. D. Swain, "Conditioning of skeletal muscle by long-term functional electrical stimulation—Implications for the development of practical systems," in *Spinal Cord Dysfunction. Vol III: Functional Stimulation*, L. S. Illis, Ed. Oxford, U.K.: Oxford University Press, 1992.

[9] R. Baratta, M. Solomonov, and G. Nguyen, "Three dimensional mapping of muscle performance for FES applications," in *Proc. Ljubljana FES Conf.*, 1993, pp. 25–26.

[10] M. Munih, K. J. Hunt, N. Donaldson, and F. M. D. Barr, "LQG moment control in the paraplegic's ankle joint," in *Proc. 18th Int. Conf. IEEE Eng. Med. Biol. Soc.*, Amsterdam, The Netherlands, 1996.

[11] N. Donaldson, F. M. D. Barr, G. F. Phillips, and T. A. Perkins, "Unsupported standing of paraplegics by stimulation of the plantarflexors: Some results from the wobbler apparatus," in *Neuroprosthetics: from Basic Research to Clinical Application*, A. Pedotti, M. Ferrarin, J. Quintern, and R. Riener, Eds. New York: Springer-Verlag, 1996.

[12] N. Donaldson, M. Munih, G. F. Phillips, and T. A. Perkins, "Apparatus and methods for studying artificial feedback-control of the plantarflexors in paraplegics without interference from the brain," *Med. Eng. Phys.*, vol. 19, pp. 525–535, 1997.

[13] A. Trnkoczy, T. Bajd, and M. Malezic, "A dynamic model of the ankle joint under functional electrical stimulation in free movement and isometric conditions," *J. Biomechan.*, vol. 9, pp. 509–519, 1978.

[14] T. J. Bajzek and R. J. Jaeger, "Characterization and control of muscle response to electrical stimulation," *Ann. Biomed. Eng.*, vol. 15, pp. 485–501, 1987.

[15] C. J. Robinson, B. Flaherty, L. Fehr, G. C. Agarwal, G. F. Harris, and G. L. Gottlieb, "Biomechanical and reflex responses to joint perturbations during electrical stimulation of muscle: Instrumentation and measurement techniques," *Med. Biologic. Eng. Comput.*, vol. 32, no. 3, pp. 261–272, 1994.

[16] T. Sinkjaer, E. Toft, S. Andreassen, and B. C. Horneman, "Muscle stiffness in human ankle dorsiflexors: Intrinsic and reflex components," *J. Neurophysiol.*, vol. 60, pp. 1110–1121, 1988.

[17] H. J. Chizeck, "Adaptive and nonlinear control methods for neural prostheses," in *Neural Prostheses*, R. B. Stein, P. H. Peckham, and D. B. Popovic, Eds. Oxford, U.K.: Oxford University Press, 1992, pp. 298–328.

[18] N. Donaldson, "Practical ankle controllers for unsupported standing in paraplegia," in *Proc. Ljubljana FES Conf.*, 1993, pp. 61–64.

[19] K. J. Hunt, M. Munih, N. Donaldson, and F. M. D. Barr, "Optimal control of ankle joint moment: Toward unsupported standing in paraplegia," *IEEE Trans. Automat. Contr.*, to be published.

[20] K. J. Hunt, M. Munih, N. Donaldson, and F. M. D. Barr, "Investigation of the Hammerstein hypothesis in the modeling of electrically stimulated muscle," *IEEE Trans. Biomed. Eng.*, to be published.

[21] M. Munih, N. Donaldson, K. J. Hunt, and F. M. D. Barr, "Feedback control of unsupported standing in paraplegia. Part II: Experimental results," *IEEE Trans. Rehab. Eng.*, this issue, p. 341–352.

[22] K. J. Hunt, "Stochastic optimal control theory with application in self-tuning control," in *Lecture Notes in Control and Information Sciences* Berlin, Germany: Springer-Verlag, 1989.

[23] V. Kučera, *Discrete Linear Control: The Polynomial Equation Approach*. New York: Wiley, 1979.

[24] H. Kwakernaak and R. Sivan, *Linear Optimal Control Systems*. New York: Wiley, 1972.

[25] K. J. Åström and B. Wittenmark, *Computer Controlled Systems: Theory and Design*, 3rd ed. Englewood Cliffs, NJ: Prentice-Hall, 1997.

[26] K. J. Åström, P. Hagander, and J. Sternby, "Zeros of sampled systems," *Automatica*, vol. 20, pp. 31–38, 1984.

[27] V. Kučera, *Analysis and Design of Discrete Linear Control Systems*. Englewood Cliffs, NJ: Prentice-Hall, 1992.

Kenneth J. Hunt received the B.Sc. degree in electrical and electronic engineering with first class honors in 1984 and the Ph.D. degree in control theory in 1987, both from the University of Strathclyde, Glasgow, Scotland, U.K.

He is a Research Scientist and Project Leader with Daimler-Benz Systems Technology Research, Berlin, Germany, part of Daimler-Benz corporate research. He is also a Visiting Professor at the Department of Automatic Control and Systems Engineering at the University of Sheffield. From 1987 to 1989, he was a Research Scientist with BBN Systems and Technologies (the European division of Bolt, Beranek and Newman, Inc. From 1989 to 1992, he held a Royal Society of Edinburgh Personal Research Fellowship, and during that period was with the Department of Mechanical Engineering at the University of Glasgow.

Marko Munih (M'88) received the B.Sc. and M.Sc. degrees in electrical engineering from the University of Ljubljana, Slovenia, in 1986 and 1989, respectively. He received the D.Sc. degree in electrical engineering in 1993 for work on controlling muscle activity with respect to the femur and tibia bone loading.

In 1989, he was Teaching Assistant at the Faculty of Electrical Engineering, Ljubljana, Slovenia. His reserch interests were focused in functional electrical stimulation of paraplegic lower extremities with surface electrode systems, including measurements, control, biomechanics and electrical circuits. From 1995 to 1996, he was a Research Assistant with the Implanted Devices Group in the Department of Medical Physics and Bioengineering at University College London, where he did research on unsupported standing of paraplegics and development of the sensory amplifier. Currently, he is a member of the Faculty of Electrical Engineering, University of Ljubljana, Slovenia.

Dr. Munih is member of the IFMBE, IFESS, and IFAC and serves as an international referee for several journals in the biomedical engineering field.

Nick de N. Donaldson received the M.A. degree in engineering from Cambridge University, Cambridge, U.K., in 1976. He received the Ph.D. degree from London University, London, U.K.

After a time spent designing integrated circuits at the General Electric Company, he joined the Medical Research Council Neurological Prostheses Unit under the direction of G. Brindley. Since then he has worked on the use of surgically implanted devices for restoring paralyzed limb function.

Since 1992, he has been Head of the Implanted Devices Group at University College London, London, U.K., which has a close collaboration with the Spinal Injuries Units at the Royal National Orthopaedic Hospital and Salisbury Hospital in England. His research interests include implant technology, implanted orthopaedic instrumentation, the biomechanics of standing, biomechanical instrumentation, nerve and nerve root stimulation, feedback control in FES, and use of ENG signals in control.

Dr. Donaldson is on the Board of Directors of IFESS.